Journal of Crystal Growth 572 (2021) 126255

Contents lists available at ScienceDirect

Journal of Crystal Growth

journal homepage: www.elsevier.com/locate/jcrysgro

# Controlled recrystallization from the melt of the organic n-type small molecule semiconductor 2-decyl-7-phenyl-[1]benzothieno[3,2-b][1]benzothiophene S,S,S′,S′-tetraoxide

Wolfgang R. Bodlos [a,*], Sara Mattiello [b], Andrea Perinot [c], Roland Fischer [d], Luca Beverina [b], Mario Caironi [c], Roland Resel [a]

[a] Institute of Solid State Physics, Graz University of Technology, Petersgasse 16, 8010 Graz, Austria
[b] Department of Materials Science, Universita di Milano-Bicocca, Via Cozzi 55, 20125 Milan, Italy
[c] Center for Nano Science and Technology@PoliMi, Istituto Italiano di Technologia, Via Pascoli 70/3, 20133 Milan, Italy
[d] Institute of Inorganic Chemistry, Graz University of Technology, Stremayrgasse 9, 8010 Graz, Austria

ARTICLE INFO

Communicated by G. Muller

ABSTRACT

Recrystallization from the melt of the n-type BTBT derivative 2-dectyl-7-phenyl-[1]benzothieno[3,2-b][1]benzothiophene S,S,S',S'-tetraoxide (Ph-BTBTOx$_2$-10) reveals a defined crystal structure of the molecule. It leads to the formation of alternating nano-segregated layers consisting of parallelly stacked aromatic units and alkyl units. This polymorph appears to be the thermodynamic stable phase. Charge carrier mobility measurements indicate an electron mobility of $4*10^{-6}$ cm$^2$ V$^{-1}$ s$^{-1}$ for this phase.

## 1. Introduction

[1]benzothieno[3,2-b][1]benzothiophene (BTBT) type molecules are among the most promising organic small molecular semiconductors to date. They connect easy synthetic access, high stability, the possibility to perform late stage functionalization and suitable solubility in a range of common processing solvents with relevant performances as organic semiconductors, particularly for use in thin film transistors.[1–6] Literature reports a wide variety of BTBT-containing derivatives, both symmetric and nonsymmetric having p-type character. $C_8$-BTBT-$C_8$ (with octyl groups at both ends) and Ph-BTBT-10 (with a phenyl unit and a decyl group at each end) are amongst the most popular symmetric and nonsymmetric derivatives [7–17]. They have shown impressive hole mobilities surpassing 5 cm$^2$ V$^{-1}$ s$^{-1}$ and highlighting how important and complex the control of molecular arrangement in the active layer by the substrate can be [13,18]. While a common approach is to use thin film deposition methods operating in the non-equilibrium regime like spin coating, physical vapor deposition or blade coating to account for metastable states, significant results have also been achieved by a more controlled crystallization. Inkjet printing, zone melting, the use of a liquid crystal precursor phases or controlled quenching from the melt are some examples [10,16,19]. In this sense Ph-BTBT-10 has shown remarkable results forming homogeneous, thermostable films [16,20–24]. We present here a slow recrystallization from the melt of an n-type BTBT derivative structurally derived from Ph-BTBT-10: 2-dectyl-7-phenyl-[1]benzothieno[3,2-b][1]benzothiophene S,S,S',S'-tetraoxide (Ph-BTBTOx$_2$-10, Fig. 1). Structural investigations are performed on thin films prepared by recrystallization from the melt by controlled cooling. A focus is given to the crystalline properties (molecular packing, preferred orientation) and it is brought into relation with the charge carrier mobility.

## 2. Experimental

The films for structural investigation were prepared onto atomically flat amorphous surfaces. As a substrate 1.5 × 1.5 cm Si wafers with a 230 ± 10 nm thermal oxide layer were used. To obtain a clean surface the substrates were rinsed with acetone and subsequently with isopropanol.

The Ph-BTBTOx$_2$-10 was synthesized directly from Ph-BTBT-10 by oxidation with m-chloroperbenzoic acid in dichloromethane solution (Supporting Information). X-ray diffraction reveals that there is more

* Corresponding author.
*E-mail addresses:* wolfgang.bodlos@tugraz.at (W.R. Bodlos), sara.mattiello@unimib.it (S. Mattiello), andrea.perinot@iit.it (A. Perinot), roland.fischer@tugraz.at (R. Fischer), luca.beverina@unimib.it (L. Beverina), mario.caironi@iit.it (M. Caironi), roland.resel@tugraz.at (R. Resel).

https://doi.org/10.1016/j.jcrysgro.2021.126255
Received 1 March 2021; Received in revised form 19 May 2021; Accepted 13 July 2021
Available online 16 July 2021

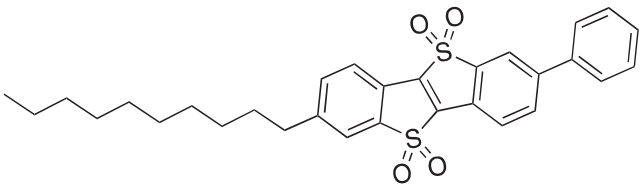

**Fig. 1.** Chemical structure of the molecule Ph-BTBTOx$_2$-10.

than one single phase present in the as-synthesized powder. The chemical structure of the molecule is shown in Fig. 1. The BTBT-Ox$_2$ core features a phenyl group and a decyl chain in the 7 and 2 position respectively. The high oxidation state of the sulfur atoms confers a particularly low lying LUMO level, an important prerequisite of semiconductors for potential n-type behavior in organic field effect transistor (OFET) structures [25–27].We have already demonstrated that Ph-BTBT-Ox$_2$-10 provides working n-channel OFET devices with mobilities in the order of $10^{-5}$ cm$^2$V$^{-1}$s$^{-1}$ for solution deposited and vacuum deposited thin films[24].

The material was probed by differential scanning calorimetry (DSC) to derive information about the phase transition behavior. The measurements were performed with 5 mg on a DCS-1 Mettler-Toledo under a $N_2$ flux of 80 ml/min from 0 to 200 °C with a heating rate of 10 K/min.

The recrystallized films for this study were prepared by distributing about 15 mg of Ph-BTBTOx$_2$-10 over the substrate surface and subjecting it to a defined heating procedure in which the melting point was carefully passed to achieve a slow recrystallisation during subsequent cooling. This was done on a DHS heating stage while purging the sample surface with Argon gas to avoid contact with air and reduce eventual evaporation of the material [28].

The films were characterized by four different X-ray based methods: specular X-ray diffraction (XRD), specular X-ray reflectivity (XRR), grazing incidence X-ray diffraction (GIXD) and single-crystal X-ray diffraction. The specular measurements (XRD & XRR) were performed on a PANalytical Empyrean diffractometer with a wavelength of $\lambda = 1.542$ Å. It is equipped with a sealed cooper tube and a multilayer mirror on the primary side and a receiving slit, a 0.02 rad Soller slit as well as a PANalytical PIXcel 3D detector on the secondary side. The transformation of the angular measurements (2θ) into reciprocal space was done by the following formula $q_z = (\frac{4\pi}{\lambda})\ \sin\theta$, with $q_z$ representing the scattering vector perpendicular to the substrate. The critical angles $\theta_c$ were determined by the incident angle at a decrease of 50% of the associated maximum intensity.

GIXD measurements were performed at the Elettra synchrotron facility on the XRD1-beamline. It was operated with a wavelength of 1.400 Å and a beam size of 200 × 200 µm. The incidence angle $\alpha_i$ was chosen at the critical angle of total external reflection $\alpha_c$ to suppress the signal from the amorphous $SiO_2$. The data was collected on a Dectris Pilatus 2 M detector and evaluated with the GIDVis software package [29]. It was used to create two-dimensional contour plots with a linearly scaled color code ranging from blue representing low intensity to yellow representing high intensity. The images were transformed to reciprocal space with $q_z$ indicating the out-of-plane part and $q_{xy}$ the in-plane part of the scattering vector.

To obtain the crystal structure solution a single crystal was removed from the surface under an optical microscope and mounted onto a glass rod on a copper pin. The crystal was cooled under a $N_2$ stream provided by an Oxford Cryosystems cryometer (T = 100 K). XRD data collection was performed on a Bruker APEX II [30] diffractometer with Mo $K_\alpha$ radiation ($\lambda = 0.7107$ Å) from an IµS microsource and an APEX II CCD area detector. Data integration was carried out using SAINT [31]. Empirical absorption corrections were applied using SADABS [32,33]. The structure was solved by the direct method [34] option in SHELXS [35] and refined by the full-matrix least-squares procedures in SHELXL [36] as implemented in the program SHELXLE [37]. All non-hydrogen atoms were refined anisotropically. All other hydrogen atoms were placed in calculated positions corresponding to standard bond lengths and angles using riding models. CIF files were edited, validated and formatted with the program Olex2 [38].

The charge carrier mobility of the films was evaluated by fabricating bottom-gate field-effect transistors with bottom contacts. Si substrates that have a thermal oxide layer of 230 ± 10 nm and pre-patterned gold source and drain contacts were used. The charge mobility was extracted from the measured transfer curves of the transistors, biased in the saturation regime at a gate ($V_g$) and drain ($V_d$) voltage of 60 V. From $V_g$, the drain current $I_d$, the channel length L and width W, and the gate dielectric capacitance $C_{diel}$ the mobility of the material was calculated from the formula $\mu_{sat} = \frac{2L}{C_{diel}W}(\frac{\partial\sqrt{I_D}}{\partial V_{GS}})^2$ [39].

## 3. Results

First insights to the phase transitions of the as-prepared powder were gained by differential scanning calorimetric measurements. The curves are given in Fig. 2, showing several endothermal processes during heating with the most intense peak at 172 °C corresponding to the melting point. By subsequent cooling, a strong exothermal reaction is observed at 155 °C assignable to the recrystallization process.

The films were thermally conditioned according to the following protocol: heating from room temperature up to 165 °C at a heating rate of 1 °C per minute; reduction of the heating rate to 0.5 °C per minute and approach of 178 °C through the melting point of 172 °C. Films were slowly cooled down from 178 to 140 °C at the rate of 0.1 °C per minute to induce a slow recrystallization allowing for structural reorganization. Finally, the samples were cooled to room temperature at a 1 °C per minute rate.

The morphology after recrystallization at room temperature is shown in Fig. 3. A rough surface with micrometer big features is visible. There appear to be different areas that differentiate in height, grain size and coverage. The substrate surface is however fully covered.

The appearing structure on the surface has a clear crystallographic order observable by X-ray diffraction. Fig. 4a shows the XRR measurements featuring strongly oscillating Kiessig fringes, two critical angles at $\theta_c = 0.23°$ ($q_z = 0.033$ Å$^{-1}$) and $\theta_c = 0.55°$ ($q_z = 0.079$ Å$^{-1}$) and several strong Bragg peaks. The fringes and the second critical angle are created by the 30 nm thick gold source drain areas of the substrate. The crystal structure of the recrystallized film creates a Bragg peak at $q_z = 0.22$ Å$^{-1}$ and its higher order diffraction peaks corresponding to a d-spacing of 28.5 Å. GIXD measurements in Fig. 4b indicate several strong intensities along Debye Scherer arcs. The crystal structure was solved by single

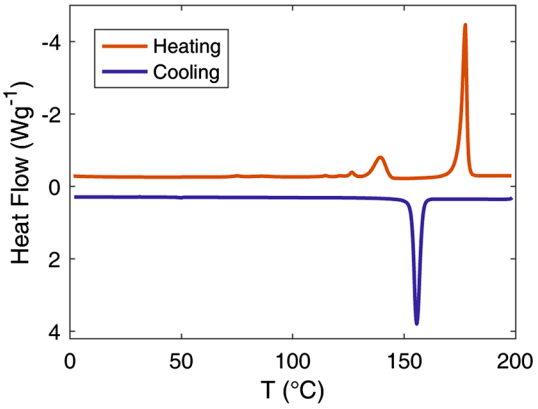


**Fig. 2.** Differential scanning calorimetry measurement of Ph-BTBTOx$_2$-10 in the powder state after synthesis. The initial heating cycle up to 200 °C (red) and subsequent cooling cycle down to 25 °C (blue) are given. (For interpretation of the references to color in this figure legend, the reader is referred to the web version of this article.)

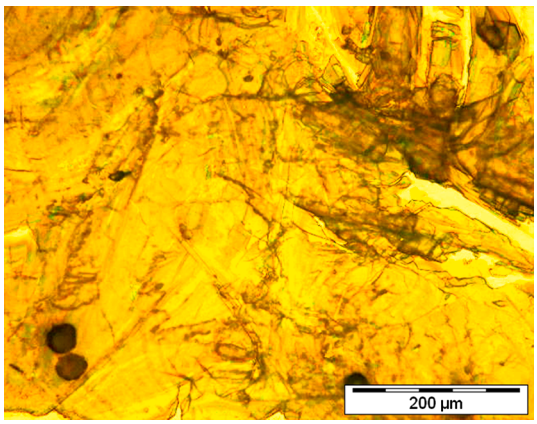


**Fig. 3.** Optical polarized microscope image of the surface morphology of a Ph-BTBTOx$_2$-10 film after recrystallization from the melt at room temperature.

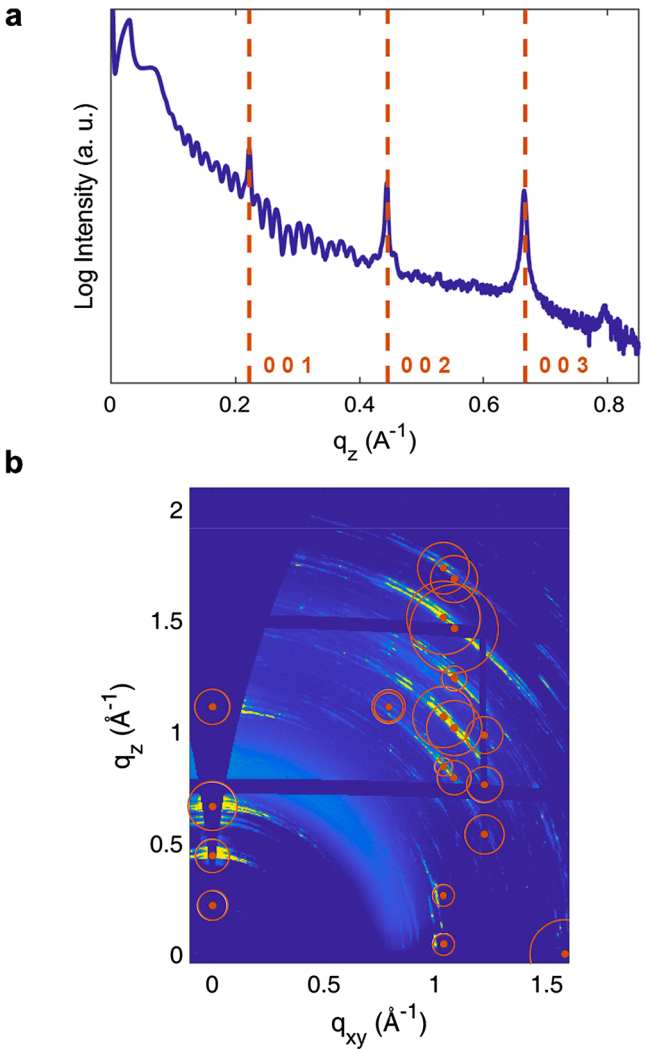


**Fig. 4.** X-ray based characterization at room temperature of a Ph-BTBTOx$_2$-10 thin film recrystallized from the melt onto a $SiO_2$ surface with embedded Au bottom gate and bottom contacts. Specular XRR measurement (a) with red dashed lines corresponding to the calculated peak positions from the crystal structure solution obtained at −173.15 °C. GIXD pattern (b) with indexed intensities represented by red dots and circles standing for the calculated peak positions and intensities (structure factor) of the crystal structure solution obtained at −173.15 °C. (For interpretation of the references to color in this figure legend, the reader is referred to the web version of this article.)

crystal X-ray diffraction at −173.15 °C. The results are summarized in Table 1 and the calculated peak positions as well as intensities from this solution are compared with the measured diffraction features at room temperature in Fig. 4 (red). The unit cell is illustrated together with the molecular packing in Fig. 5a (left). The molecules take a zig-zag arrangement towards each other with the head and tail groups forming a kink of 86°. Looking at the general packing, the molecules take a head-to-head and tail-to-tail arrangement forming alternating nano-segregated layers of alkyl units and aromatic core units. The alkyl chains interdigitate in their respective layers and minimize thereby the space towards each other. The crystals orient with the crystallographic (0 0 1) plane parallel to the substrate as shown in Fig. 5a (right) giving the aromatic cores an inclination angle of 35° and leading to a π orbital stacking distance of ~ 3.4 Å.

The electrical characteristics from mobility measurements in OFETs are shown in Fig. 6. The thin film transistors show an n-type behavior, with a turn on at an applied gate voltage $V_g$ of about 17 V ($V_d$ = 60 V) with a reasonably low gate leakage ($I_g$) compared to the channel current (I). The extracted saturation electron mobility is very modest, it shows a $V_g$ dependence, reaching a plateau above ~ 30 V, corresponding to an average value of $4*10^{-6}$ cm$^2$ V$^{-1}$ s$^{-1}$. The transfer curve measurements suggest the presence of trapping effects at the interface with the dielectric or in the bulk layer, which is expected due to the poly-crystalline nature of the film apparent in Fig. 3. Traps can be formed not only at the interface with the dielectric but also on the interfaces between different crystallites. The value is however consistent with what we observed for solution and vacuum processed films in a similar configuration [25].

## 4. Discussion

Ph-BTBTOx$_2$-10 shows a characteristic melting and recrystallization behavior on $SiO_2$ surfaces. During slow recrystallization from the melt, a crystal structure with a defined molecular packing appears. This phase is not present in the as-synthesized powder. The molecules orient with the aromatic cores and the (0 0 1) plane towards the surface taking an inclination angle of 35°. The π - π stacking distance of the aromatic cores is thereby around 3.4 Å.

Previous studies on Ph-BTBTOx$_2$-10 revealed a rather disordered structure after thin film deposition with cold crystallization taking place at elevated temperatures [25].

Recrystallization from the melt however, leads to a completely different phase. The unit cell and the orientation of the molecules within the cell is very distinct as shown in Fig. 5. The aromatic cores and alkyl chains are less strongly inclined towards each other in the recrystallized phase and don't alternate in orientation. A comparison of the mass densities of the two phases (1.249 $\frac{g}{cm^3}$ and 1.310 $\frac{g}{cm^3}$) reveals a

**Table 1**
Crystal data and structure refinement.

| | |
|---|---|
| **CCDC** | 2,057,319 |
| **Empirical formula** | $2(C_{15}H_{16}O_2S)$ |
| **Formula weight** | 520.67 |
| **Temperature / K** | 99.98 |
| **Crystal system** | triclinic |
| **Space group** | P-1 |
| **a/Å** | 8.0766(6) |
| **b/Å** | 11.7708(9) |
| **c/Å** | 28.3455(18) |
| **α/°** | 84.905(3) |
| **β/°** | 88.967(3) |
| **γ/°** | 79.508(4) |
| **Volume/Å$^3$** | 2639.2(3) |
| **Z** | 4 |
| **$\rho_{calc}$ g/cm$^3$** | 1.310 |
| **Crystal size/mm$^3$** | 0.41 × 0.24 × 0.04 |
| **Final R indexes [I>=2σ (I)]** | $R_1$ = 0.0541, $wR_2$ = 0.1062 |
| **Final R indexes [all data]** | $R_1$ = 0.1057, $wR_2$ = 0.1260 |

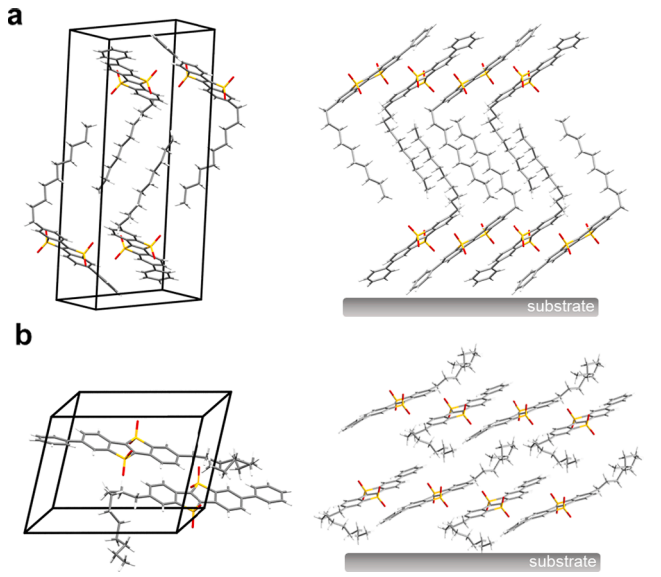


**Fig. 5.** Packing of the molecules within the crystallographic unit cell (left) and the arrangement of the molecules across layers relative to the substrate surface (right) for the recrystalized phase (a) and a known polymorph (b) [25].

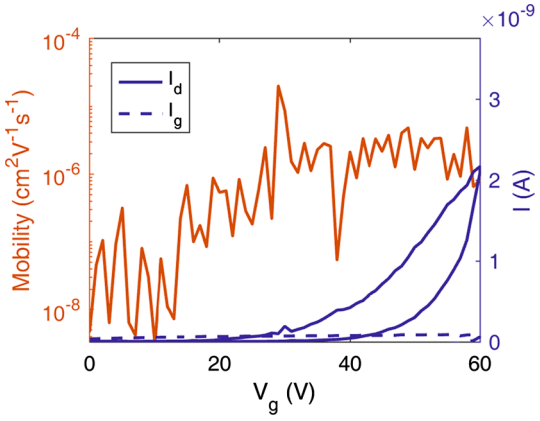


**Fig. 6.** Charge transport mobility of a recrystallized film from the melt of the molecule BTBT-$Ox_2$ measured in a bottom gate - bottom contact configuration in the saturation regime together with the transfer characteristic measured at $V_d = V_g = 60$ V.

considerable higher density after recrystallization from the melt. This provides certain evidence that the recrystallized phase is closer to thermodynamic equilibrium. The observation of so distinct phases under different preparation conditions strongly emphasizes the role of polymorphism as an important design consideration. [40]

Charge carrier mobility measurements indicate an electron mobility of $4*10^{-6}$ $cm^2$ $V^{-1}$ $s^{-1}$ in the saturation regime. It is lower compared to the previously studied Ph-BTBT$Ox_2$-10 polymorph. Considering the density difference, this is in accordance with a common observation that metastable phases often have a better performance. [40,41]

The rather low charge transport mobility in thin film transistors for both phases can originate from different reasons besides a low general intrinsic mobility of Ph-BTBT$Ox_2$-10 itself. It is often influenced by the high energetic barrier for the electron injection into the LUMO level using high work function metals and the tendency of electrons to get trapped at the dielectric interface or trapping centers (impurities or grain boundaries). [39]

## 5. Conclusion

Structural investigations on thin films of the asymmetric n-type Ph-BTBT$Ox_2$-10 prepared by recrystallization from the melt show a specific crystal structure and molecular packing with a full surface coverage. It has a triclinic unit cell with a 001 orientation towards the substrate in which the head and tail groups take a zig zag arrangement towards each other, leading to a head-to-head and tail-to-tail stacking of the molecules. Alternating nano-segregated segments consisting of aromatic core layers and interdigitated decyl chain layers are formed with the former in contact with the substrate. The charge carrier transport measurements indicate an electron mobility of $4*10^{-6}$ $cm^2$ $V^{-1}$ $s^{-1}$. This polymorph is thermodynamically more stable than the already known phase formed by thin film growth but it has a lower charge carrier mobility.

## 6. Appendices

### Supporting Information

The Supporting Information is available free of charge.
Synthesis of the Molecule.

## 7. Accession Codes

CCDC 2,057,319 contains the supplementary crystallographic data. It can be obtained free of charge from The Cambridge Crystallographic Data Centre via www.ccdc.cam.ac.uk/structures.

## 8. Funding sources

This project was financed by the Austrian Science Fund (project P30222).

## CRediT authorship contribution statement

**Wolfgang R. Bodlos:** Conceptualization, Methodology, Investigation, Writing – original draft. **Sara Mattiello:** Investigation, Writing - review & editing. **Andrea Perinot:** Investigation, Writing - review & editing. **Roland Fischer:** . **Luca Beverina:** Investigation, Writing - review & editing. **Mario Caironi:** Investigation, Writing - review & editing. **Roland Resel:** Conceptualization, Methodology, Investigation, Writing – original draft.

## Declaration of Competing Interest

The authors declare that they have no known competing financial interests or personal relationships that could have appeared to influence the work reported in this paper.

## Appendix A. Supplementary material

Supplementary data to this article can be found online at https://doi.org/10.1016/j.jcrysgro.2021.126255.

## References

[1] H. Ebata, T. Izawa, E. Miyazaki, K. Takimiya, M. Ikeda, H. Kuwabara, T. Yui, Highly Soluble [1]Benzothieno[3,2- *b* ]Benzothiophene (BTBT) Derivatives for High-Performance, Solution-Processed Organic Field-Effect Transistors, J. Am. Chem. Soc. 129 (51) (2007) 15732–15733, https://doi.org/10.1021/ja074841i10.1021/ja074841i.s00310.1021/ja074841i.s004.

[2] T. Izawa, E. Miyazaki, K. Takimiya, Molecular Ordering of High-Performance Soluble Molecular Semiconductors and Re-Evaluation of Their Field-Effect Transistor Characteristics, Adv. Mater. 20 (18) (2008) 3388–3392, https://doi.org/10.1002/adma.200800799.

[3] I. McCulloch, M. Heeney, C. Bailey, K. Genevicius, I. MacDonald, M. Shkunov, D. Sparrowe, S. Tierney, R. Wagner, W. Zhang, M.L. Chabinyc, R.J. Kline, M. D. McGehee, M.F. Toney, Liquid-Crystalline Semiconducting Polymers with High Charge-Carrier Mobility, Nature Mater. 5 (4) (2006) 328–333, https://doi.org/10.1038/nmat1612.

[4] K. Takimiya, S. Shinamura, I. Osaka, E. Miyazaki, Thienoacene-Based Organic Semiconductors, Adv. Mater. 23 (38) (2011) 4347–4370, https://doi.org/10.1002/adma.201102007.

[5] C. Niebel, Y. Kim, C. Ruzié, J. Karpinska, B. Chattopadhyay, G. Schweicher, A. Richard, V. Lemaur, Y. Olivier, J. Cornil, A.R. Kennedy, Y. Diao, W.-Y. Lee, S. Mannsfeld, Z. Bao, Y.H. Geerts, Thienoacene Dimers Based on the Thieno[3,2-b] Thiophene Moiety: Synthesis, Characterization and Electronic Properties, J. Mater. Chem. C 3 (3) (2015) 674–685, https://doi.org/10.1039/C4TC02158D.

[6] C. Wang, H. Dong, W. Hu, Y. Liu, D. Zhu, Semiconducting π-Conjugated Systems in Field-Effect Transistors: A Material Odyssey of Organic Electronics, Chem. Rev. 112 (4) (2012) 2208–2267, https://doi.org/10.1021/cr100380z.

[7] T. Uemura, Y. Hirose, M. Uno, K. Takimiya, J. Takeya, Very High Mobility in Solution-Processed Organic Thin-Film Transistors of Highly Ordered [1] Benzothieno[3,2-b]Benzothiophene Derivatives, Appl. Phys. Exp. 2 (11) (2009) 111501, https://doi.org/10.1143/APEX.2.111501.

[8] Y. Tsutsui, G. Schweicher, B. Chattopadhyay, T. Sakurai, J.-B. Arlin, C. Ruzié, A. Aliev, A. Ciesielski, S. Colella, A.R. Kennedy, V. Lemaur, Y. Olivier, R. Hadji, L. Sanguinet, F. Castet, S. Osella, D. Dudenko, D. Beljonne, J. Cornil, P. Samorì, S. Seki, Y.H. Geerts, Unraveling Unprecedented Charge Carrier Mobility through Structure Property Relationship of Four Isomers of Didodecyl[1]Benzothieno[3,2- *b* ][1]Benzothiophene, Adv. Mater. 28 (33) (2016) 7106–7114, https://doi.org/10.1002/adma.v28.3310.1002/adma.201601285.

[9] M. Dohr, H.M.A. Ehmann, A.O.F. Jones, I. Salzmann, Q. Shen, C. Teichert, C. Ruzié, G. Schweicher, Y.H. Geerts, R. Resel, M. Sferrazza, O. Werzer, Reversibility of Temperature Driven Discrete Layer-by-Layer Formation of Dioctyl-Benzothieno-Benzothiophene Films, Soft Matter. 13 (12) (2017) 2322–2329, https://doi.org/10.1039/C6SM02541B.

[10] H. Minemawari, T. Yamada, H. Matsui, J. Tsutsumi, S. Haas, R. Chiba, R. Kumai, T. Hasegawa, Inkjet Printing of Single-Crystal Films, Nature 475 (7356) (2011) 364–367, https://doi.org/10.1038/nature10313.

[11] G. Schweicher, V. Lemaur, C. Niebel, C. Ruzié, Y. Diao, O. Goto, W.-Y. Lee, Y. Kim, J.-B. Arlin, J. Karpinska, A.R. Kennedy, S.R. Parkin, Y. Olivier, S.C.B. Mannsfeld, J. Cornil, Y.H. Geerts, Z. Bao, Bulky End-Capped [1]Benzothieno[3,2- *b* ] Benzothiophenes: Reaching High-Mobility Organic Semiconductors by Fine Tuning of the Crystalline Solid-State Order, Adv. Mater. 27 (19) (2015) 3066–3072, https://doi.org/10.1002/adma.v27.1910.1002/adma.201500322.

[12] G.H. Roche, Y.-T. Tsai, S. Clevers, D. Thuau, F. Castet, Y.H. Geerts, J.J.E. Moreau, G. Wantz, O.J. Dautel, The Role of H-Bonds in the Solid State Organization of [1] Benzothieno[3,2-b][1]Benzothiophene (BTBT) Structures: Bis(Hydroxy-Hexyl)-BTBT, as a Functional Derivative Offering Efficient Air Stable Organic Field Effect Transistors (OFETs), J. Mater. Chem. C 4 (28) (2016) 6742–6749, https://doi.org/10.1039/C6TC01814A.

[13] A.O.F. Jones, B. Chattopadhyay, Y.H. Geerts, R. Resel, Substrate-Induced and Thin-Film Phases: Polymorphism of Organic Materials on Surfaces, Adv. Funct. Mater. 26 (14) (2016) 2233–2255, https://doi.org/10.1002/adfm.v26.1410.1002/adfm.201503169.

[14] A.O.F. Jones, Y.H. Geerts, J. Karpinska, A.R. Kennedy, R. Resel, C. Röthel, C. Ruzié, O. Werzer, M. Sferrazza, Substrate-Induced Phase of a [1]Benzothieno[3,2- *b* ] Benzothiophene Derivative and Phase Evolution by Aging and Solvent Vapor Annealing, ACS Appl. Mater. Interf. 7 (3) (2015) 1868–1873, https://doi.org/10.1021/am5075908.

[15] R. Janneck, N. Pilet, S.P. Bommanaboyena, B. Watts, P. Heremans, J. Genoe, C. Rolin, Highly Crystalline C8-BTBT Thin-Film Transistors by Lateral Homo-Epitaxial Growth on Printed Templates, Adv. Mater. 29 (44) (2017) 1703864, https://doi.org/10.1002/adma.201703864.

[16] H. Iino, T. Usui, J. Hanna, Liquid Crystals for Organic Thin-Film Transistors, Nat. Commun. 6 (1) (2015) 6828, https://doi.org/10.1038/ncomms7828.

[17] C. He, Y. He, X. Liu, A. Li, J. Chen, H. Meng, Enhancing the Performance of Solution-Processed Organic Thin-Film Transistors by Blending Binary Compatible Small Molecule Semiconductors, Organic Electronics 64 (2019) 104–109, https://doi.org/10.1016/j.orgel.2018.10.009.

[18] M. Mas-Torrent, C. Rovira, Role of Molecular Order and Solid-State Structure in Organic Field-Effect Transistors, Chem. Rev. 111 (8) (2011) 4833–4856, https://doi.org/10.1021/cr100142w.

[19] J.M. Adhikari, K. Vakhshouri, B.D. Calitree, A. Hexemer, M.A. Hickner, E. D. Gomez, Controlling Crystallization to Improve Charge Mobilities in Transistors Based on 2,7-Dioctyl[1]Benzothieno[3,2-b][1]Benzothiophene, J. Mater. Chem. C 3 (34) (2015) 8799–8803, https://doi.org/10.1039/C5TC01253H.

[20] J. Cho, T. Mori, Low-Temperature Band Transport and Impact of Contact Resistance in Organic Field-Effect Transistors Based on Single-Crystal Films of Ph-BTBT-C10, Phys. Rev. Appl. 5 (6) (2016), 064017, https://doi.org/10.1103/PhysRevApplied.5.064017.

[21] Y.-F. Wang, H. Iino, J. Hanna, Fabrication of Planarly-Oriented Polycrystalline Thin Films of Smectic Liquid Crystalline Organic Semiconductors, Soft Matter. 13 (37) (2017) 6499–6505, https://doi.org/10.1039/C7SM01303E.

[22] H. Iino, J. Hanna, Liquid Crystalline Organic Semiconductors for Organic Transistor Applications, Polym. J. 49 (1) (2017) 23–30, https://doi.org/10.1038/pj.2016.101.

[23] S. Inoue, H. Minemawari, J. Tsutsumi, M. Chikamatsu, T. Yamada, S. Horiuchi, M. Tanaka, R. Kumai, M. Yoneya, T. Hasegawa, Effects of Substituted Alkyl Chain Length on Solution-Processable Layered Organic Semiconductor Crystals, Chem. Mater. 27 (11) (2015) 3809–3812, https://doi.org/10.1021/acs.chemmater.5b00810.

[24] H. Minemawari, M. Tanaka, S. Tsuzuki, S. Inoue, T. Yamada, R. Kumai, Y. Shimoi, T. Hasegawa, Enhanced Layered-Herringbone Packing Due to Long Alkyl Chain Substitution in Solution-Processable Organic Semiconductors, Chem. Mater. 29 (3) (2017) 1245–1254, https://doi.org/10.1021/acs.chemmater.6b04628.

[25] W.R. Bodlos, S. Mattiello, A. Perinot, L. Gigli, N. Demitri, L. Beverina, M. Caironi, R. Resel, Cold Crystallization of the Organic N-Type Small Molecule Semiconductor 2-Decyl-7-Phenyl-[1]Benzothieno[3,2- *b* ][1]Benzothiophene S, S, S′ S′-Tetraoxide, Crystal Growth Des. 21 (1) (2021) 325–332, https://doi.org/10.1021/acs.cgd.0c01157.

[26] G. Mattioli, S. Mattiello, M. Sassi, L. Beverina, Ab Initio Simulations of Interfaces between SAM-Modified Gold Electrodes and n-Type or p-Type Organic Semiconductors Based on the Benzothieno-Benzothiophene (BTBT) Architecture, J. Phys. Chem. C 124 (6) (2020) 3601–3609, https://doi.org/10.1021/acs.jpcc.9b0965410.1021/acs.jpcc.9b09654.s001.

[27] S. Mattiello, A. Sanzone, F. Bruni, M. Gandini, V. Pinchetti, A. Monguzzi, I. Facchinetti, R. Ruffo, F. Meinardi, G. Mattioli, M. Sassi, S. Brovelli, L. Beverina, Chemically Sustainable Large Stokes Shift Derivatives for High-Performance Large-Area Transparent Luminescent Solar Concentrators, Joule 4 (9) (2020) 1988–2003, https://doi.org/10.1016/j.joule.2020.08.006.

[28] R. Resel, E. Tamas, B. Sonderegger, P. Hofbauer, J. Keckes, A Heating Stage up to 1173 K for X-Ray Diffraction Studies in the Whole Orientation Space, J. Appl. Crystallogr. 36 (1) (2003) 80–85, https://doi.org/10.1107/S0021889802019568.

[29] B. Schrode, S. Pachmajer, M. Dohr, C. Röthel, J. Domke, T. Fritz, R. Resel, O. Werzer, *GIDVis* : A Comprehensive Software Tool for Geometry-Independent Grazing-Incidence X-Ray Diffraction Data Analysis and Pole-Figure Calculations, J. Appl. Crystallogr. 52 (3) (2019) 683–689, https://doi.org/10.1107/S1600576719004485.

[30] APEX2. APEX2. Bruker AXS Inc. Madison, Wisconsin, (USA) 2012.

[31] SAINT. SAINT. Bruker AXS Inc. Madison, Wisconsin, (USA) 2012.

[32] R.H. Blessing, An Empirical Correction for Absorption Anisotropy, Acta Crystallograph. Sec. A Found. Crystallogr. 51 (1) (1995) 33–38, https://doi.org/10.1107/S0108767394005726.

[33] Sheldrick, G. M.; SADABS. SADABS - Program for Empirical Absorption Correction of Area Detector Data. University of Göttingen, Germany 1996.

[34] G.M. Sheldrick, Phase Annealing in SHELX-90: Direct Methods for Larger Structures, Acta Crystallogr. Sec. A 46 (6) (1990) 467–473, https://doi.org/10.1107/S0108767390000277.

[35] Sheldrick, G. M.; SHELXS97. SHELXS97. University of Göttingen, Germany 1997.

[36] G.M. Sheldrick, Crystal Structure Refinement with SHELXL, Acta Crystallogr. Sec. C Struct. Chem. 71 (1) (2015) 3–8, https://doi.org/10.1107/S2053229614024218.

[37] C.B. Hübschle, G.M. Sheldrick, B. Dittrich, ShelXle: A Qt Graphical User Interface for SHELXL, J. Appl. Cryst. 44 (2011) 1281–1284.

[38] O.V. Dolomanov, L.J. Bourhis, R.J. Gildea, J.A.K. Howard, H. Puschmann, OLEX2: A Complete Structure Solution, Refinement and Analysis Program, J. Appl. Crystallogr. 42 (2) (2009) 339–341, https://doi.org/10.1107/S0021889808042726.

[39] Z.A. Lamport, H.F. Haneef, Sajant Anand, Matthew Waldrip, O.D. Jurchescu, Tutorial: Organic Field-Effect Transistors: Materials, Structure and Operation, J. Appl. Phys. 124 (7) (2018) 071101, https://doi.org/10.1063/1.5042255.

[40] H. Chung, Y. Diao, Polymorphism as an Emerging Design Strategy for High Performance Organic Electronics, J. Mater. Chem. C 4 (18) (2016) 3915–3933, https://doi.org/10.1039/C5TC04390E.

[41] D. Nabok, P. Puschnig, C. Ambrosch-Draxl, O. Werzer, R. Resel, D.-M. Smilgies, Crystal and Electronic Structures of Pentacene Thin Films from Grazing-Incidence x-Ray Diffraction and First-Principles Calculations, Phys. Rev. B 76 (23) (2007), 235322, https://doi.org/10.1103/PhysRevB.76.235322.